# Texture mapping in electron beam welded dissimilar Copper-Stainless steel joints by Neutron diffraction

Soumitra Kumar Dinda[1*], Jyotirmaya Kar[2], Gour Gopal Roy[2], Winfried Kockelmann[3], Prakash Srirangam[4]

[1]Materials Science and Engineering, University of Toronto, Canada

[2]Metallurgical and Materials Engineering, Indian Institute of Technology Kharagpur, India

[3]STFC-Rutherford Appleton Laboratory, ISIS Facility, UK

[4]Warwick Manufacturing Group (WMG), University of Warwick, UK

*Corresponding author: soumitra.dinda@utoronto.ca, Canada, Tel: +1 647-656-8248

In this study, the crystallographic texture variation of electron beam welded dissimilar copper to 304L stainless-steel joints was investigated using Time-of-flight neutron diffraction measurements. The effect of beam oscillation by changing its oscillation diameter on texture orientation variation was evaluated. Neutron diffraction measurements were performed using General Materials Diffractometer beamline at Rutherford Appleton Laboratory neutron radiation source. Phase fractions and variations of crystallographic texture in terms of pole figures and inverse pole figures were obtained. The stronger texture we found in all regions of the joints i.e. heat-affected zone and fusion zone for oscillating beam compared to its non-oscillating counterparts. Also, by increasing the oscillation diameter, from its optimum value, a weaker texture was found, which had a detrimental effect on mechanical properties. Electron-backscatter diffraction texture measurements were also performed to compare and complement the results obtained from neutron texture.

*Keywords: Electron beam welding; Dissimilar metal welds; Stainless steel - Copper welds; Beam oscillation; Neutron diffraction; Bulk texture.*

The dissimilar joining of copper (Cu) to stainless steel (SS) is one such joint which finds applications in the field of power generation, heat transfer components, nuclear sector, and cryogenic sectors [1,2]. This type of joint is designed to provide excellent thermal and electrical conduction from Cu and strength, wear and corrosion resistance, imparted by SS [3]. Fusion welding of Cu to SS by conventional fusion welding is challenging due to the differences in physical, chemical and thermo-mechanical properties and limited solid solubility [4]. Electron beam welding (EBW) is a fusion welding process that yields good mechanical and metallurgical properties in comparison to other welding techniques [5,6] and offers specific advantages like high power density, high depth to width ratio and fewer defects formation [7]. During welding, weld metal undergoes through the complicated thermal cycle and liquid flow which significantly affects the microstructure and mechanical properties within the fusion zone (FZ) that could be influenced by grains orientation and texture formation [8]. Different conventional non-destructive techniques like X-Ray, electron backscatter diffraction (EBSD) have already been performed for weld texture study. With comparison to this, neutron diffraction has the ability to penetrate thick metals approximately 1 $cm^3$ (for steel) which provides the unique possibility to study bulk textural properties and coarse-grained materials as well as the texture of fine-grained materials with excellent grains statistics [9,10]. Joints performance not only associated with the surface but solely depends on bulk properties which can be explained by bulk texture. Using a polychromatic beam and with many detectors at fixed scattering angles, time of flight (TOF) neutron diffraction has some considerable advantages for texture analysis since significant portions of both reciprocal and orientation space are simultaneously covered in one measurement. Texture variation of different regions of the joints examined by different researchers by different techniques like EBSD, hard X-ray of materials like different SS, Al-alloys, Ti-alloys [11–14]. Few researchers also worked for other weld systems like steel, Zr-alloys with high energy polychromic neutron beam [15–17]. In

this publication, we report the texture study of EB-welded Cu-SS joints under different weld conditions of all regions of the joints and EBSD was also performed for one joint for comparison with neutron results.

Cu and AISI-304L SS plates were selected for the EB-welding by taking as beam oscillation is the variable parameter and joints prepared, i.e. Joint 1 (without oscillation), Joint 2 (1.0 mm oscillation diameter) and Joint 3 (2mm oscillation diameter). Other processing parameters kept in fixed during the experiments. Neutron diffraction measurements were performed using the general materials diffractometer (GEM) with dimensions of 100 x 10 x 3 $mm^3$ cut from the full welded joints and selected five points having both base metals (BMs), both heat-affected zone (HAZ) and FZ. The wavelength range maintained here 0.2 to 3.5 Å with a beam size of 5 x 15 $mm^2$. Data sets were analysed by Extended-WIMV (E-WIMV) algorithm with orientation distribution function (ODF) cell size of $10^o$ [18]. Due to joints absorption anisotropy and to control the displacement effects on both structure and texture, list of parameters were refined i.e., both sample displacement, TOF absorption coefficient, monitor counts and backgrounds [19]. *Figure 1* displays three diffraction patterns for Joint-1 for both BMs and FZ showing different diffraction peaks. One or two FCC phases were observed and within the FZ, very weak BCC peaks also found. Lattice parameters were refined for major phases where significant Bragg peak was observed and was kept fixed for minor phases, like for Cu (3.615 Å) in the SS HAZ and SS (3.609 Å) in the Cu HAZ with constant Debye-Waller parameter value of 0.8 $Å^2$. MTEX [20] in Matlab was used to obtain final pole figures (PFs) and inverse pole figures (IPFs) of all joints. EBSD analysis of Joint 1 was performed perpendicular to the weld direction of all regions of the joints to discuss the differences and similarities with neutron results.

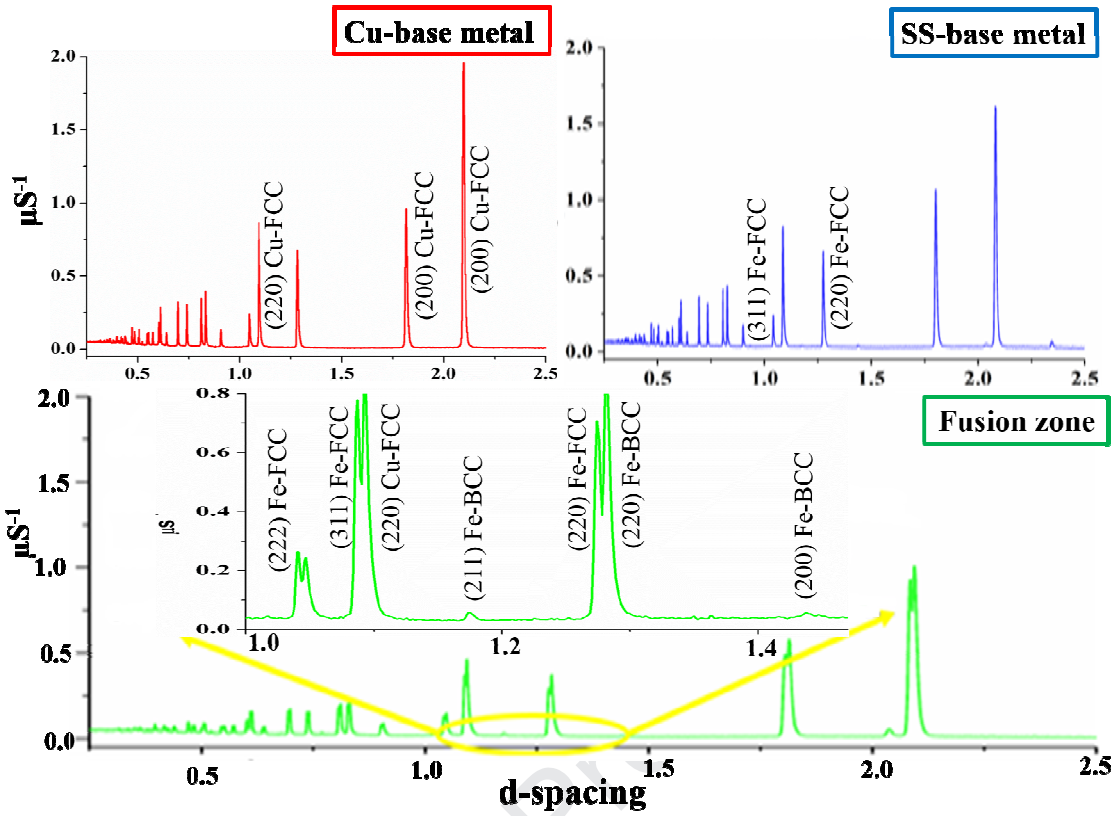


***Figure 1.*** Diffraction patterns of Joint 1 showing for both BMs and fusion zone respectively.

The IPFs from EBSD results (*Figure 2*) of each BM shows fewer planes are oriented along 111 & 101 II ND for Cu compared to SS. For Cu, the maximum grains are found with 001 oriented II ND, and minimum along 101, 111 II ND whereas for SS, maximum grains are along 111, 101 II ND and minimum along 100 II ND. For the Cu HAZ region, maximum planes of both Cu FCC phases and SS FCC phase-oriented along 100 & 101 II ND and very less along 111 II ND but in FZ, the maximum grains are along 111 & 101 II ND and very few grains along 100 II ND for both phases as similar obtained from SS-HAZ and SS BM regions. EBSD results show basic ideas about the changes of crystallographic orientation for FZ and HAZ in comparison with BMs due to thermal process involved during welding. Bulk texture presented here in terms of PFs and IPFs by considering three non-collinear planes (111), (200) and (220) or its parallel planes.

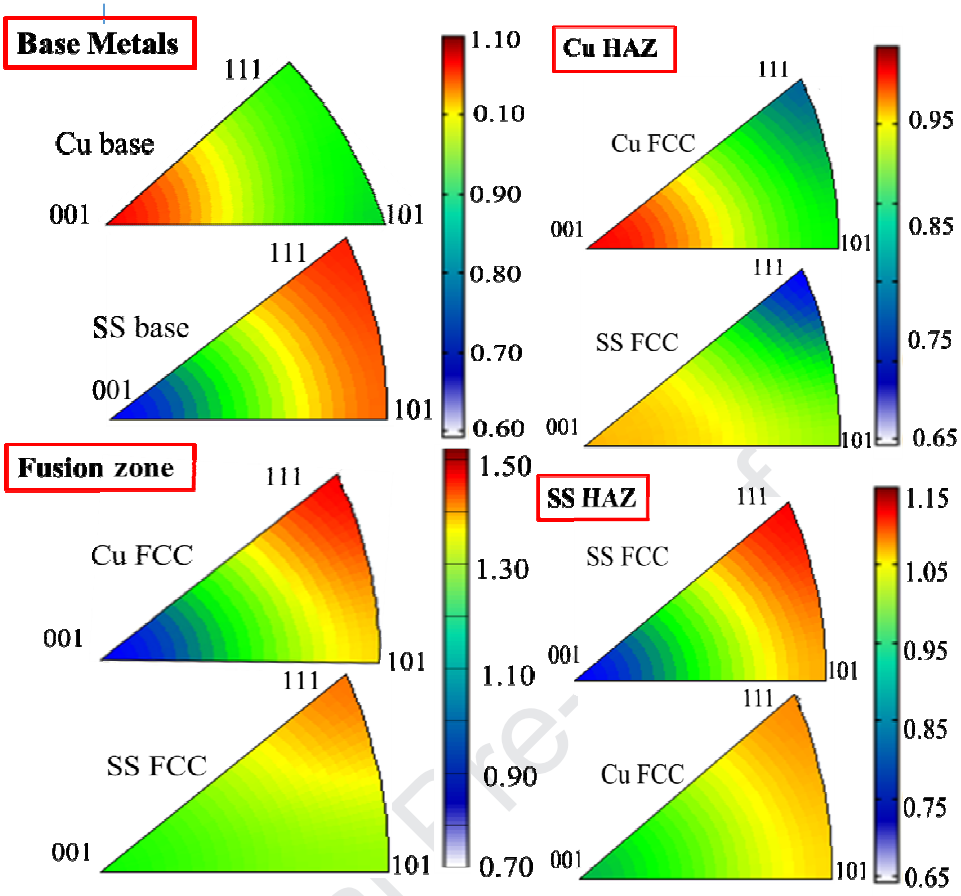


***Figure 2.*** IPFs from EBSD results of Joint 1 in ND for all regions.

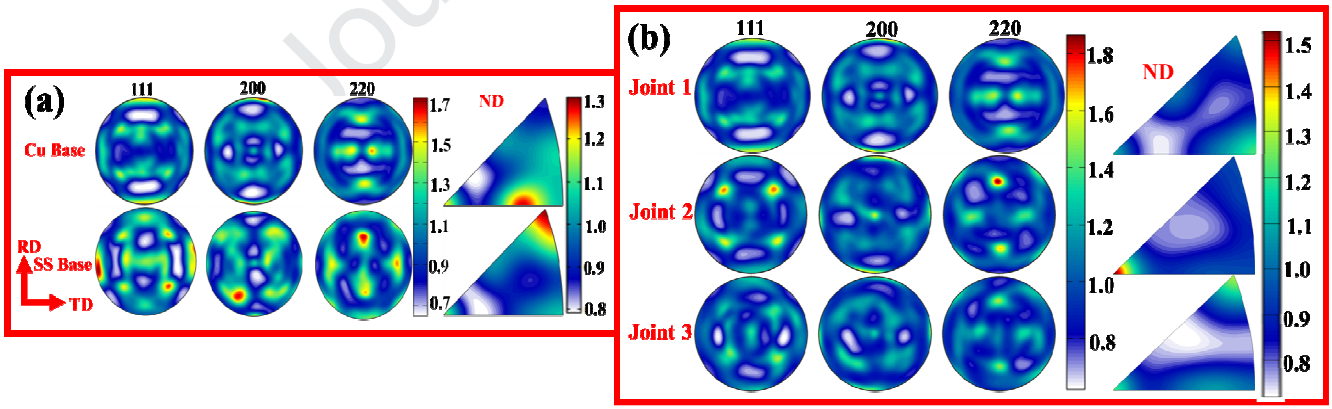


***Figure 3.*** (a) PFs & IPFs of both BMs & (b) Cu phase in Cu-HAZ. N.B. all are in the same m.r.d.

*Figure 3(a)* shows the similar characteristics of the BMs as presented from EBSD study i.e. Cu-base showing major grains oriented along 112, 010 II ND which gives less deformation due to less in slip systems whereas SS-base shows the easy movement of dislocation due to the presence of

more closed pack slip systems (more 111, 110 II ND) [21]. *Figure 3(b)* shows the variation for Cu HAZ region. In contrast with *Figure 3(a),* the PFs & IPFs in both HAZ shows significantly different texture. It is clear for every case, type and appearance of texture are quite similar, but pole densities are different. Joint 2 showing much stronger pole densities along 100 & 010 II ND where other two joints show the increased probability for 111 II ND & on average along 100, 112 II ND. *Table 1* in Cu HAZ shows, limiting diffusion of steel take place in every case due to the limited solid solubility of Cu into steel. We assume that the Cu-HAZ includes small regions of the SS-FCC phase that have a small number of SS-FCC crystallites. Hence Bragg reflections for SS-FCC are may present at a few angles but not present in all diffraction detectors which was why the Rietveld fit returned a zero-phase fraction overall. *Figure 4(a)* shows PFs and IPFs of Cu phase of Joint 1 in FZ and it shows that the pole densities are higher along in 110 & 111 II ND where and less along 100 II ND whereas in case of Joint 2, maximum pole densities are along 111, 112 & 110 II ND and very less along 100 & 311 II ND compared to Joint 1. For Joint 3 systems, we observed more mixed type texture orientation compared to the other two joints. *Figure 4(b)* shows for SS phase in FZ and Joint 1, found more pole densities along 211, 100 & 210 II ND and moderate along 111 II ND as compared to Joint 2 where maximum densities are along 111, 110 & 112 and moderate along in 100 II ND and as similar obtained for Joint 3 also. *Table 1* in FZ shows phase fractions and found more steel phase for Joint 3 (61 %) compared to Joint 2 (51%) and lowest for Joint 1 (41%), however, this could be a misalignment effect of the neutron beam on the sample but Joint 2 shows a more homogeneous distribution of both alloying elements i.e. Cu (48%) and SS (51%) that helps to provide better properties. Joint 3 shows more alloying distribution within FZ but not in homogeneously distributed. It forms chunks or agglomerated Cu precipitates that is not recommended. In every case, we found a small component of the SS-BCC

phase, which is delta ferrite that is mainly formed at a high temperature at SS-HAZ and FZ during the solidification.

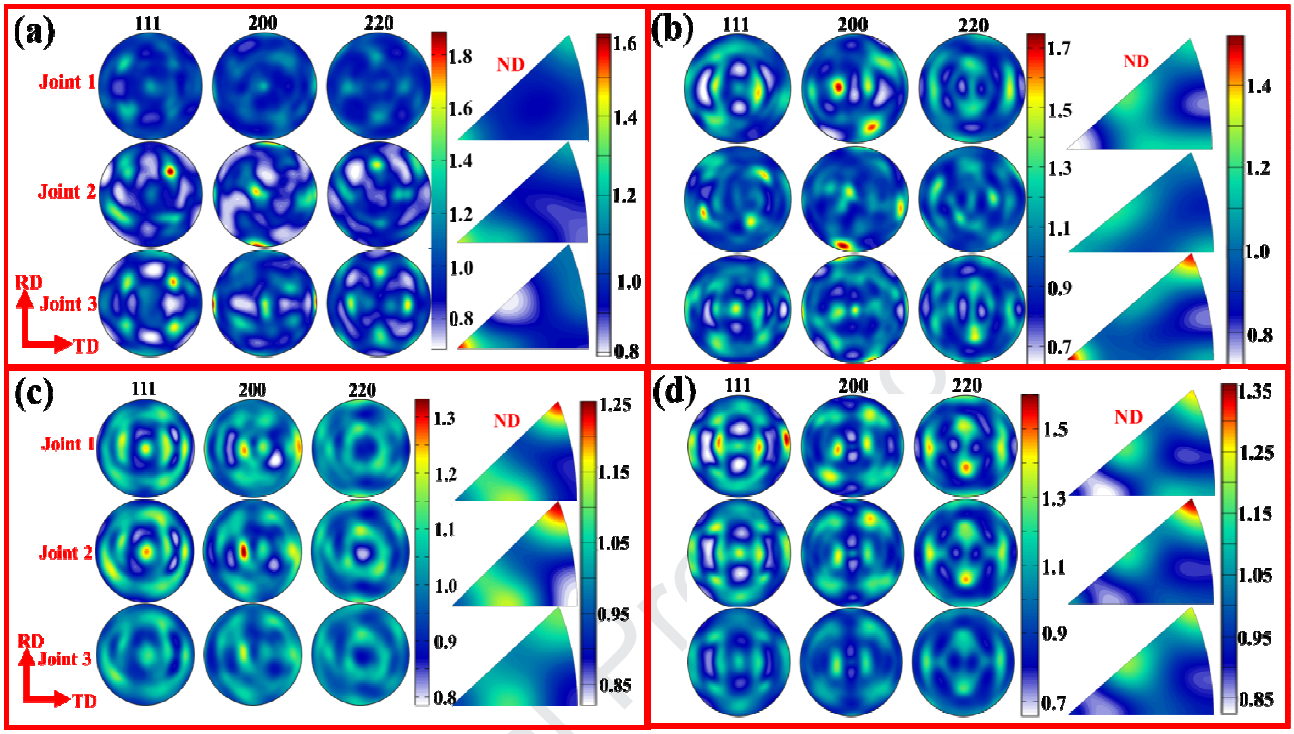


***Figure 4*** PFs & IPFs of ***(a)*** Cu & ***(b)*** SS phase in FZ, ***(c)*** Cu & ***(d)*** SS phase in SS HAZ. N.B. all are in the same m.r.d.

Whereas *Figure 4(c)* presents for Cu-FCC phase in SS-HAZ region as a minor phase. Here, for Joint 3, no stronger pole densities are observed in comparison with the other two joints. Joint 1 & 2 have similar trends with a majority of pole densities oriented along 111, 211 & 210 II ND. *Figure 4(d)* shows for SS-FCC phase in this SS-HAZ region. For Joint 3, maximum pole densities are along 211 & 111 II ND and in between along 111 II ND but less strong compared to Joint 2 which has better dislocation movements compared to Joint 1. The last column from *Table 1* shows for SS-HAZ regions information and found that Cu diffusion took place into steel and it varies on welding processing condition. A very little amount of delta ferrite is also found in this HAZ area.

Table 1: Details PFs comparison among all regions of all joints.

| Joints | Phases | Cu-HAZ | Fusion zone | SS-HAZ |
|---|---|---|---|---|
| | Phases name | Phase % | Phase % | Phase % |
| Joint 1 | Cu-FCC | 99.999 | 57.31 | 17.59 |
| | SS-FCC | 0.0001 | 41.34 | 79.43 |
| | SS-BCC | - | 1.35 | 2.98 |
| Joint 2 | Cu FCC | 99.999 | 47.98 | 11.78 |
| | SS-FCC | 0.0001 | 50.59 | 86.95 |
| | SS-BCC | - | 1.43 | 1.27 |
| Joint 3 | Cu-FCC | 99.999 | 37.65 | 11.02 |
| | SS-FCC | 0.0001 | 60.98 | 88.84 |
| | SS-BCC | - | 1.37 | 0.13 |

From our observation, it's clear that much intense and stronger pole densities (111, 112 & 110 II ND for FCC phase) are observed in case of Joint 2 which was prepared by the oscillating beam at 1 mm diameter compared to Joint 1 (without oscillation) and weakest orientation for Joint 3 (2 mm oscillation diameter). *Table 1* shows that the major melting occurred on the steel-side whereas limiting or restricted melting took place on the Cu-side due to very high thermal conductivity of Cu. As a result, a large amount of heat dissipated from Cu to steel takes place. Another reason may be due to the limited solid solubility of steel in Cu. For other side HAZ (SS-HAZ), found a little bit of Cu-FCC phase (10-17%). Authors previous work [22] by microstructural and mechanical studies, shows that the oscillating beam (1mm diameter) produced more uniform and homogeneous microstructure by a homogeneous distribution of Cu in FZ plays an important role for getting best joints properties. Authors also made the hypothesis [22] on beam oscillation by discussing the churning action fundamentals which provides more oriented and aligns texture in

both FZ and HAZ. Other reason is that the beam oscillation creates repeated melting and solidification of the same small tiny weld bead leads to reduce its overall cooling rate. Further increase in oscillation diameter from its optimum value, the weld pool might be so small that the fractional overlapping much lower that may cause a lower degree of mixing. Compared to EBSD (Joint 1), neutron diffraction shows a similar trend of results but for bulk texture study, neutron study gives more promising results throughout the joints thickness. The following conclusions can be drawn from our study.

Cu to 304L stainless-steel dissimilar joining was carried out using the EB-welding process under both oscillating and non-oscillating beam by varying its diameter for TOF neutron diffraction bulk texture study. Optimum oscillating diameter (1mm) yields a region of relatively ordered texture in preferred orientation at both heat-affected and fusion zone compared to its non-oscillating counterparts by proper elemental mixing due to homogenous and uniform weld microstructure. More oscillating diameter from its optimum value seems to produce joints having more randomized texture with fewer intensities which are not recommended for properties as justified by previous mechanical studies.



[1] C. Lusch, M. Börsch, C. Heidt, N. Magginetti, J. Sas, K.P. Weiss, S. Grohmann, IOP Conference Series: Materials Science and Engineering. 102 (2015).

[2] M. Turna, M. Sahul, J. Ondruska, J. Lokaj, International DAAAM Symposium. 22 (2011) 833–834.

[3] J. Kar, S.K. Dinda, G.G. Roy, S.K. Roy, P. Srirangam, Vacuum. 149 (2018) 200–206.

[4] Y. Zhang, J. Huang, H. Chi, N. Cheng, Z. Cheng, S. Chen, Materials Letters. 156 (2015) 7–9.

[5] D. Wang, H. Wang, H. Cui, G. He, Materials Processing Technology. 237 (2016) 277–285.

[6] S.K. Dinda, P. Srirangam, G.G. Roy, The TMS Society (2019) 239–249.

[7] B. Bandi, S.K. Dinda, J. Kar, G.G. Roy, P. Srirangam, Vacuum. 158 (2018) 172–179.

[8] W. Han, S. Ukai, F. Wan, Y. Sato, B. Leng, H. Numata, N. Oono, S. Hayashi, Q. Tang, Y. Sugino, Materials Transactions. 53 (2012) 390–394.

[9] A.S. Tremsin, S. Ganguly, S.M. Meco, G.R. Pardal, T. Shinohara, W.B. Feller, Applied Crystallography. 49 (2016) 1130–1140.

[10] S.K. Dinda, W. Kockelmann, G.G. Roy, P. Srirangam, International Journal of Advanced Manufacturing Technology. 108 (2020) 1499-1508.

[11] E. Maawad, W. Gan, M. Hofmann, V. Ventzke, S. Riekehr, H.-G. Brokmeier, N. Kashaev, M. Müller, Materials & Design. 101 (2016) 137–145.

[12] A. Eghlimi, M. Shamanian, M. Eskandarian, A. Zabolian, J.A. Szpunar, Materials Characterization. 106 (2015) 208–217.

[13] H.-G. Brokmeier, S. Lenser, R. Schwarzer, V. Ventzke, S. Riekehr, M. Kocak, J. Homeyer, THERMEC 2006. 539–543 (2007) 3894–3899.

[14] S. Sharma, M. Turski, M. Fitzpatrick, IASMiRT (2011) 6–11.

[15] R.R. Hosbons, E.F. Ibrahim, T.M. Holden, J.H. Root, ASM nternational 28 (1989) 103–106.

[16] Y. Tomota, Science and Technology of Advanced Materials. 20 (2019) 1189–1206.

[17] J.H. Root, A. Salinas-Rodriguez, Textures and Microstructures. 14 (1991) 989–994.

[18] H.-R. Wenk, L. Lutterotti, S.C. Vogel, Powder Diffraction. 25 (2010) 283–296.

[19] W. Kockelmann, L.C. Chapon, P.G. Radaelli, Physica B: Condensed Matter. 385-386 I (2006) 639–643.

[20] M. List, U. Guide, F. Overview, MTEX Toolbox (/), (2018).

[21] C. Wang, Materials Engineering. (2014) 174–206.

[22] J. Kar, S.K. Roy, G.G. Roy, Materials Processing Technology. 233 (2016) 174–185.